JOM, Vol. 68, No. 12, 2016
DOI: 10.1007/s11837-016-2031-x

Study of Porosity on Titania Slag Obtained by Conventional Sintering and Thermal Plasma Process

S. SAMAL[1,2,3,4]

1.—The Centre for the Development of Engineering Research, VÚTS, a.s., 461 01 Liberec, Czech Republic. 2.—University of Rennes 1, 350 65 Rennes, France. 3.—e-mail: samasneha@gmail.com. 4.—e-mail: samal.sneha-manjaree@univ-rennes1.fr

This article investigates the development of porosity in titania-rich slag obtained by sintering via conventional and thermal plasma heating at 1000°C in inert atmosphere. The holder in the plasma reactor acted as the discharge anode confined within a hollow graphite cathode. Quantitative evaluation of the porosity in the conventionally sintered and plasma-sintered titania-rich slag was performed via pycnometry. Specifically, the physical dimension and morphology of the pores were characterized according to the area fraction, mean diameter, shape factor, and elongation factor. Under both conventional and thermal plasma heating conditions, porosity developed on the surface of titania-rich slag. The titania-rich slag obtained by two processes showed different porosity features in terms of the morphology and porosity. A lower porosity was observed in the plasma-sintered sample when compared with that obtained via conventional heating.

INTRODUCTION

Ilmenite ($FeTiO_3$) is a black mineral with a high content of iron oxide in the form of Fe_2O_3 and FeO and titanium in the form of TiO_2. Plasma heating is commonly employed for the melting of ilmenite at high temperatures. Most properties of sintered ilmenite are strongly related to its porosity, pore dimension, and morphology. The latter characteristics can be used as indicative parameters to evaluate and regulate the sintering process. Pores or voids are commonly formed in both plasma-treated materials and materials heated by conventional means in a furnace. Thus, the pore amount and morphology greatly contribute to the actual physical properties of the resulting products. Typically, during plasma heating, the thermal plasma melts the raw material, and the molten material cools naturally in air. The resulting material features pores of various shapes and forms, such as interlamellar, globular, and irregular pores. Such pores are generated owing to imperfect contact and partially molten particles or gas entrapment.[1,2] Currently, numerous methods are used for porosity measurement such as digital image analysis,[3] Brunauer–Emmett–Teller (BET) model,[4] Archimedean displacement, and small-angle neutron scattering (SANS). The digital image analysis quantifies porosity (i.e., the average volume fraction of porosity) by image analysis of cross-section views of the average surface fraction. The accuracy of this method depends significantly on the metallographic preparation. The BET method measures porosity gravimetrically by filling the material with either a gas or a liquid and obtaining the volume of the pores from the mass of the adsorbed fluid. This procedure assumes a constant absorbate density throughout the pore system.[5] Nevertheless, in microporous and ultramicroporous materials, wherein the surface area-to-volume ratio is very high, the influence of the pore walls on the packing of gas or liquid molecules may not be negligible, thus, leading to potential systematic errors in the evaluations. Moreover, both aforementioned methods fail to measure open pores accurately. The Archimedean displacement measures porosity by recording mass variations. Yet, this method is limited by the accuracy of the measured mass loss and difficulty in estimating the matrix density when allotropic transformation occurs. The SANS method can be used to characterize porosity by collecting information on specific void surface areas of ceramic deposits. Nonetheless, a previous study has shown poor dependency between the specific void surface area and mechanical properties of deposit materials.[6] Furthermore, the

(Published online July 27, 2016)

volumetrically averaged information used in the SANS-based model is not representative of the real material microstructure. Among all methods discussed, the image analysis method is the most widely employed owing to its reproducibility, cost effectiveness, simplicity, and versatility for analysis and characterization of porosity.[7,8]

In this work, image analysis and pycnometry were employed to evaluate the porosities of titania-rich slag obtained by both conventionally sintering and the thermal plasma process. The effects of three factors (i.e., roughness of the polished surface, magnification, and number of fields of view) on the porosity of ilmenite sintered by the earlier methods were studied. Finally, the optimized values for the three parameters were suggested based on the experimental results and comparative analysis conducted.

EXPERIMENTAL

Ilmenite [supplied by Indian Rare Earths (OSCOM), Ltd, Chatrapur; composition TiO_2: 50.5, FeO: 34.2, Fe_2O_3: 12.2, Al_2O_3: 0.45, SiO_2: 0.80, MgO: 0.75, MnO: 0.55, and Y_2O_5: 0.22] was subjected to conventional heating (in a furnace) and thermal plasma heating to study the development of surface porosity and surface morphology in the resulting materials of titania-rich slag. For the conventional heating process, pellets of ilmenite with thicknesses of 0.5 mm and diameters of 5 mm were prepared in UTS (ultra tensile strength) at a pressure of 20 Pa. Polyvinyl alcohol was used as a binder for compaction of ilmenite powder to form the pellets. The pellets were then heated in argon atmosphere in a graphite furnace at ~1000°C for 120 min. For the thermal plasma treatment, an ilmenite powder sample was treated in argon plasma for 2 min at 10 kW and 1000°C.

The morphological features of the conventionally sintered and plasma-sintered ilmenite were studied by optical microscopy and scanning electron microscopy (SEM JEOL JSM 35CF).[9] The pores were analyzed using image analysis techniques. Additionally, the shape and elongation factors of the generated cracks were determined.

For the characterization studies, the sintered samples were sectioned and impregnated into epoxy resin under vacuum to minimize pore distortion during metallographic preparation; the latter involved hand-based techniques.[10] Image acquisition was performed on nonetched samples us-ing a digital camera (Nikon's new DXM 1200 digital camera) coupled to an optical microscope (Microscopy, A-10), with magnifications in the range of 100–800×, in gray scale, and a resolution of 2088 × 1550 pixels (i.e., 574 × 246 μm^2). For each sample, 5–10 images were acquired for the pore calculations. The image analysis software Analysis 6.1 (Image-Pro Plus version, 6.0.0.260) was used for the quantitative analysis of the pores. Besides the area fraction, three parameters were measured to characterize the dimension and morphology of the pores further:[11,12] (I) pore diameter, d (μm); (II) shape factor, $f_{shape} = 4\pi(d_{min}/2)^2$; and (III) elongation factor, $f_{elong} = d_{min}/d_{max}$.

Parameters d_{min} and d_{max} are the minimum and maximum pore diameters. Parameters of f_{shape} and f_{elong}, of which the values range between 0 and 1, describe different pore charac-teristics as illustrated in Fig. 1. Parameter f_{shape} depends on both the geometrical form and the contour regularity of the pore (Fig. 1a). A f_{shape} of 1 is associated with a uniform circumference. Parameter f_{elong} indicates the elongation level of the pores, independently of the contour; for ellipsoidal pores, $f_{elong} < 1$ and for spherical pores, $f_{elong} = 1$, as illustrated in Fig. 1b. The porosity was obtained by calculating the area fraction of the pores related to the total area of the image. The results are an average value of eight or more images. Quantification of titania-rich slag images was performed by analyzing all the pores as well as the large pores only. For the larger pores, the number of large pores corresponding to 10% of the total number was considered. The size and morphology of the pores were determined by taking the average value of the pore distribution for all pores in each sample. The results are an arithmetic average of ten medians measured for each sample.

RESULTS AND DISCUSSION

Figure 2 shows the different pores present in titania-rich slag obtained by sintering and the plasma-sintered ilmenite sample. Both the pore size and the shape, from circular to elliptical forms, varied. Specifically, Fig. 2a revealed the presence of cracks and some pores on the surface of the plasma-sintered ilmenite. In contrast, the ilmenite sample, heated in a furnace below the melting temperature of ilmenite, featured fragmented particles with various cracks on its surface (Fig. 2b). It is believed that cracks form initially before forming larger cavities on the surface of the ilmenite particles. The bigger particles on the edge of titania-rich slag fragmented into smaller particles.

Further comparison of the development of pores in the conventionally sintered and plasma-sintered ilmenite revealed that the thermal plasma treatment influenced the surface of the obtained minerals. A considerably larger quantity of pores was observed in the conventionally sintered ilmenite. In contrast, the plasma-sintered ilmenite featured fewer pores on the surface of Ti-rich slag.[13]

More specifically, spherical pores were more prominently observed in the plasma-sintered sample when compared with elliptical pores. Consequently, the sample featured a pore elongation factor of less than 1. And the sample featured a pore shape factor of 1 owing to the spherical nature of the pores (Figs. 3 and 4). The error bars in the graphs represent standard deviations of the

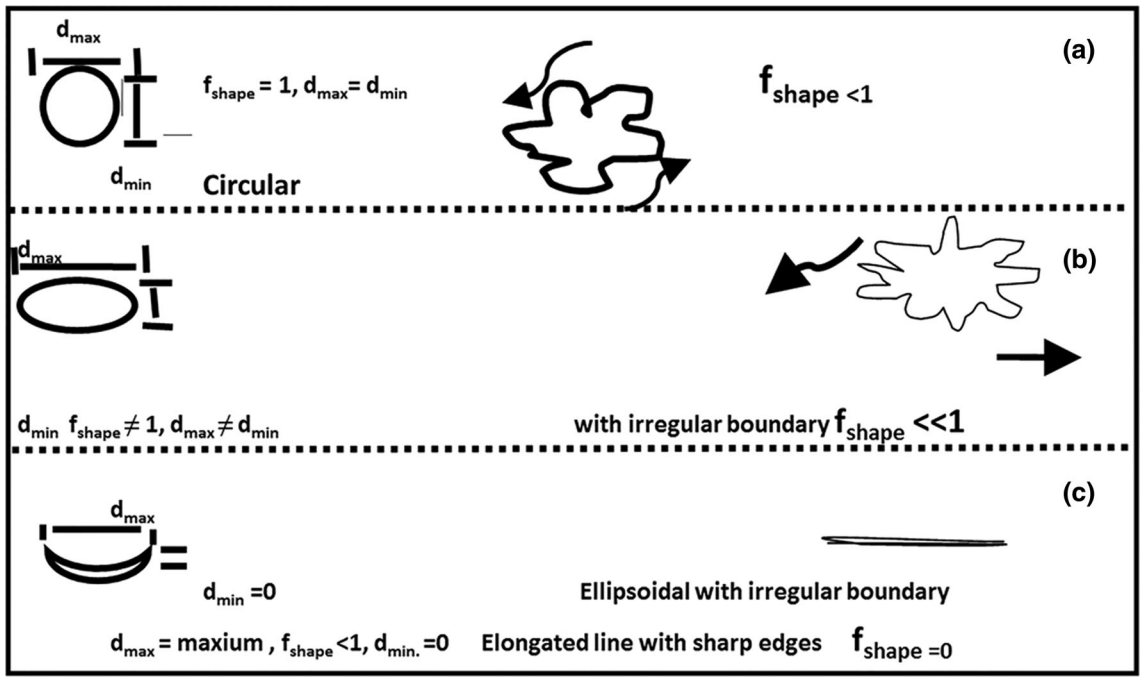

Fig. 1. Schematic representation of various shape factors of pore (a) spherical shape (very sharp boundary), (b) elliptical shape (elongated shape), and (c) very irregular shape (rough boundary).

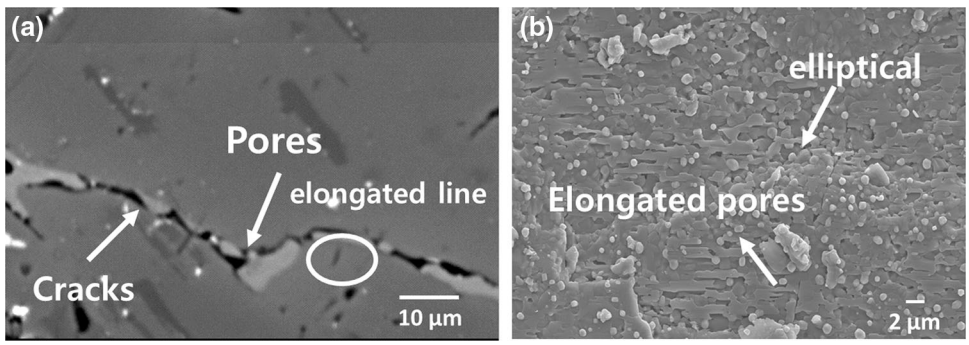

Fig. 2. SEM-SEI of the sintered ilmenite is showing the pososity in various ranges from spherical to elliptical ranges: (a) plasma-sintered ilmenite showing cracks obtained from thermal plasma reactor and (b) the sintered ilmenite, surface morphology showing the pores after treating inside the conventional heating process.

porosity data. The shape and elongation factors as a function of pore diameter are presented in Figs. 5 and 6. As observed, the shape factor increased to a maximum of 1, whereas the elongation factor displayed an opposite trend.

In contrast, elliptical pores tend to develop during conventional sintering of ilmenite in a furnace. The elongation factor for the pores was 1. By comparison, fewer spherical pores were observed. Consequently, the shape factor was less than 1. Figure 7 shows the shape factor and elongation factor of the conventionally sintered ilmenite as a function of pore diameter. Unlike the results obtained in Figs. 5 and 6, the elongation factor displayed a positive correlation with the pore diameter, whereas the spherical factor deviated from the standard behavior.

A Ti-rich slag sample was examined for comparison because the thermal plasma product is obtained from the same precursor (ilmenite). Cracks were observed on the surface of the plasma-treated sample. In contrast, the sample heated in a furnace did not feature any cracks. As discussed, the sintered ilmenite showed the opposite trend. These results indicated that the effects of sintering in ilmenite are less pronounced when compared with those in Ti-rich slag during sintering in a furnace. Thus, the sintering of Ti-rich slag in a furnace is more efficient than that of ilmenite.

High-resolution image analysis is necessary to examine samples more efficiently, especially thin cracks. The key element for the porosity measurement in sample is needed for analysis of microstructural images for pore size and

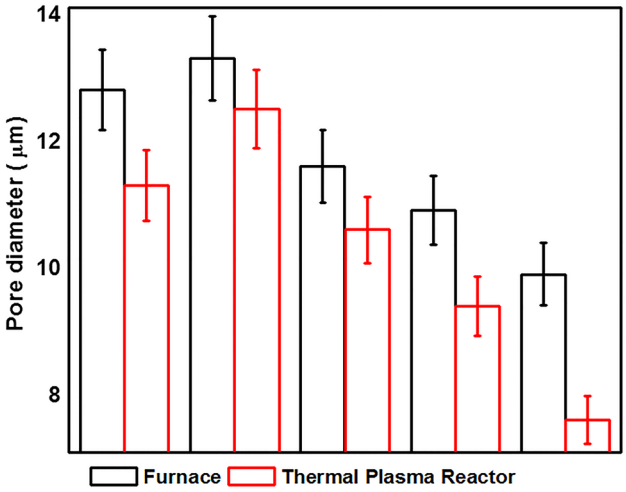

Fig. 3. Pore diameter as a function of furnace and thermal plasma reactor with standard error bars.

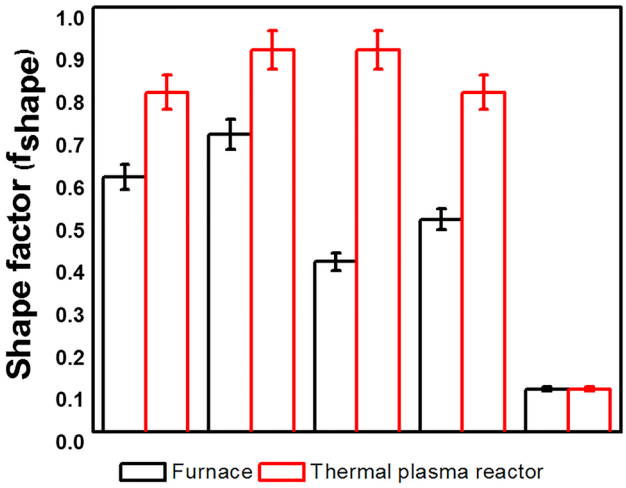

Fig. 4. Shape factor of pores inside furnace and thermal plasma reactor with standard error bars.

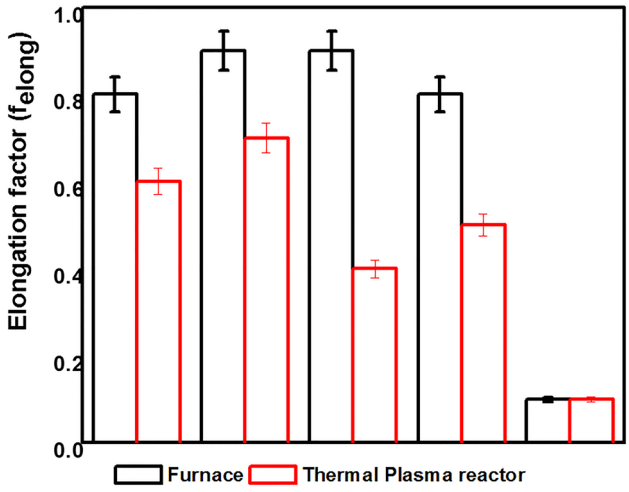

Fig. 5. Elongation factor of pores inside furnace and thermal plasma reactor with standard error bars.

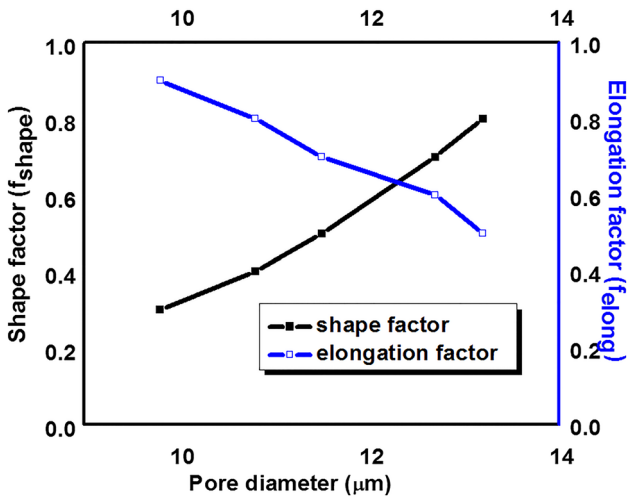

Fig. 6. Pore diameter in the function of shape factor and elongation factor for the thermal plasma reactor.

distribution. Therefore, selecting an appropriate sample area to extract maximum information on the pores of a sample is important. By using a low-magnification image analysis, the amount of porosity is determined in quantity. For higher magnification analyses, it is necessary to collect more images to obtain a standard and stable value of pore shape and diameter. At a lower magnification, a larger sample area can be examined so that various levels of porosity can be observed. Under the same magnification, it was observed that the sample heated in a furnace featured more pores than the sample treated in a thermal plasma reactor. Figure 8a and b shows the interlamellar pores and cracks, which remained unresolved at lower magnification. These images were obtained with an optical microscope. Figure 8c and d shows that the path for crack elongation originated at the pores and that the cracks spread toward the

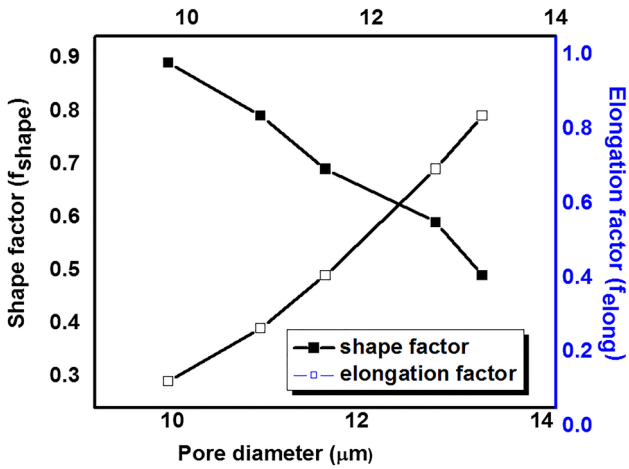

Fig. 7. Pore diameter in the function of shape factor and elongation factor inside the furnace.

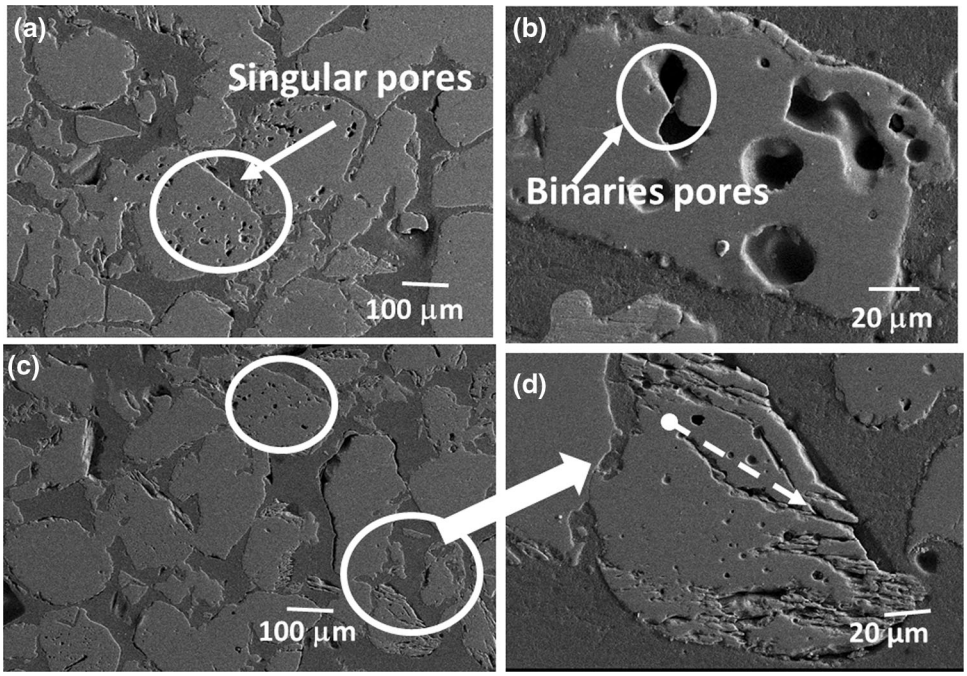

Fig. 8. SEI presentation of titania-rich slag inside the graphite resistive furnace: (a) The sample shows that the spherical pores on the surface area; (b) adjoining between two different pores are observed here; (c) lower magnification shows on different areas; and (d) one grain shows line cracks that initiate from a single pore.

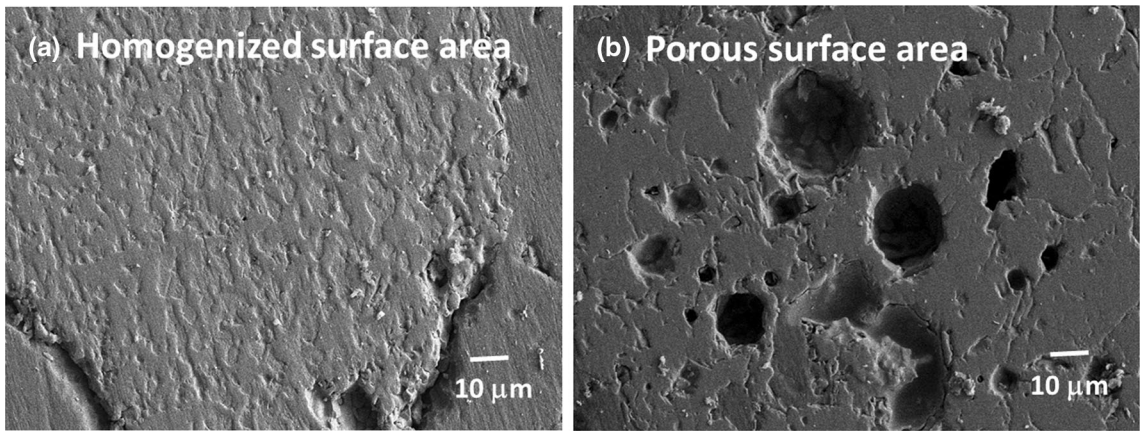

Fig. 9. (a) SEI presentation of ilmenite after sintering inside the thermal plasma and (b) resistive graph furnace.

boundary or edge of the sample. The measured porosity data were based on average values with the associated deviation ranges. The deviation ranges were wider when the data reliability was higher. Furthermore, the deviation range was narrower when more sample areas of observations were examined. Under different magnifications, when various numbers of field views were chosen, the deviation became large. These results indicate that at a proper reliability, fewer fields of view are required at a lower magnification. Additionally, choosing a proper magnification is necessary to examine more fields of views, thereby generating a more reliable porosity measurement with a narrow range of deviation. Additionally, collecting more micrographs is necessary for obtaining a reliable porosity measurement with a narrow deviation. Concurrently, fewer data points can result in a stabilized deviation, which appears more promptly for lower-magnification analysis and agrees with the experimental results. Figure 9a and b shows ilmenite after sintering in the thermal plasma process and conventional sintering in the resistive graphite furnace. The results show the presence of

spherical pores near the boundary of the sample, with various elliptical pores observed throughout the surface.

CONCLUSION

A comparative study of the porosity, pore dimension, and morphology of ilmenite and Ti-rich slag sintered inside a furnace and thermal plasma reactor was performed. The determination of the mean diameter of pores, based on the shape factor and the elongation factor, was appropriate for characterizing the porosity and individual dimension and morphology of the pores. As observed in the literature and the current study, the shape factor is the most important parameter for characterizing the evolution of pores or crack morphology during sintering. More precise results could be obtained with lower surface roughness and more fields of views at higher magnification. Finally, the average porosity data showed good correlation behaviors with the shape and elongation factors for the sintering techniques examined. Better predications regarding the microstructure analysis of materials subjected to conventional heating in a furnace and plasma heating can be made. Samples sintered inside a thermal plasma reactor have fewer pores when compared with those sintered in a furnace.

ACKNOWLEDGEMENTS

The author would like to thankful the Centre for the Development of Engineering Research, VÚTS, a.s., Liberec XI, Czech Republic, for the financial and technical support of the publication of this work.

REFERENCES

1. H. Du, J.H. Shin, and S.W. Lee, *J. Therm. Spray Technol.* 14, 453 (2005).
2. H.C. Pavanati, A.M. Maliska, A.N. Klein, and J.L.R. Muzart, *Mater. Res.* 10, 87 (2007).
3. R.M. German, *Sintering Theory and Practice* (New York: Wiley, 1996).
4. W.F. Gale and T.C. Totemeier, *Smithells Metals Refrence Book*, 8th ed. (Oxford: Butterworth Heinemann, 2004).
5. B.L. Ferguson and O.D. Smith, in *Metals Handbook*, vol. 7, Powder Metallurgy, 9th edn. (ASM, Metals Park, OH, 1984), pp. 537–541.
6. F. Tümmler and R. Oberacker, *Introduction to Powder Metallurgy* (The Institute of Materials: Cambridge, 1993).
7. Z. Wang, A. Kulkarni, S. Deshpanda, T. Nakamura, and H. Herman, *Acta Mater.* 51, 5319 (2003).
8. A. Kulkarni, A. Vaidya, A. Goland, S. Sampath, and H. Herman, *Mater. Eng. A* 359, 100 (2003).
9. S. Samal, *JOM* 2, 1 (2016).
10. K. Geels, D.B. Fowler, W-.U. Kopp, M.U. Kopp, and M. Rückert Rückert, *Metallographic and Materialographic Specimen Metallographic and Materialographic Specimen Preparation, Light Microscopy, Image Analysis and Hardness Testing* (ASTM International, West Conshohocken, PA, 2007), p. 479.
11. C.-J. Li and A. Ohmori, *J. Therm. Spray Technol.* 11, 365 (2002).
12. S.J. Dapkunas, *J. Therm. Spray Technol.* 6, 67 (1997).
13. S. Samal, B.K. Mohapatra, P.S. Mukherjee, and S.K. Chatterjee, *J. Alloys Compd.* 47, 484 (2009).